International Journal of Applied and Natural Sciences (IJANS)
ISSN(P): 2319-4014; ISSN(E): 2319-4022
Vol. 6, Issue 2, Feb – Mar 2017; 47-60

International Academy of Science, Engineering and Technology
Connecting Researchers; Nurturing Innovations

Zn CONCENTRATION INFLUENCE ON THE STRUCTURE, MORPHOLOGY AND MAGNETIC PROPERTIES OF $Co_{(1-X)}Zn_XFe_2O_4$ NANOPARTICLES IN FERROFLUIDS

J. LOPEZ[1], W. R. AGUIRRE-CONTRERAS[2], M. E. GÓMEZ[3] & G. ZAMBRANO[4]

[1,3,4]Thin Film Group, Physics Department, Universidad del Valle, Cali, Colombia

[1]CONACYT - Centro de Nano ciencias y Nanotecnología, Universidad Nacional Autónoma de México, Apdo. Postal 14, Ensenada B.C – México

[2]Grupo de Metalurgia Física y Transiciones de Fase, Universidad del Valle, Departamento de Física, Cali, Colombia

ABSTRACT

Ferro fluids based on a single domain of $Co_{(1-x)}Zn_xFe_2O_4$ magnetic nanoparticles with a mean diameter of approximately 15 nm dispersed in toluene as a liquid carrier were prepared. The samples were characterized using scanning electron microscopy (SEM), X-ray diffraction (XRD) and vibrating sample magnetometer (VSM). XRD patterns show the formation of a spinel structure and allowed to determine the mean size of the crystallite of nanoparticles from the Rietveld refinement results, shows that it is diminished from 33 to 20 nm when the Zn concentration increases from 0.25 to 0.75. The magnetic hysteresis loops for the magnetic samples exhibit superparamagnetic behavior, from which it was established that the coercive field decreases while the saturation magnetization M_s increases with the increase of Zn at %. This magnetic behavior may be due to the partial substitution of non-magnetic Zn^{+2} ions that occupy tetrahedral interstitial sites and thereby change the cation distribution in the spinel structure and can affect the magnetic moment alignment in the samples. Additionally, using the Thamm–Hesse analysis, we could establish that the magnetization change values, ΔM (B), are close to zero for the highest magnetic field, indicating that the existing interaction favors the super paramagnetic behavior of the magnetic nanoparticles in the ferrofluid. This result has been predicted by the Stoner–Wolfforth model for a system with a set of single domain-uniaxial anisotropy and non-interacting small magnetic particles. The above result shows that our magnetic nanoparticles are materials with potential applications in nanotechnology for developing magnetically tunable devices.

KEYWORDS: Magnetic nanoparticles, Ferro fluids, Thamm–Hesse Analysis, Superparamagnetism

INTRODUCTION

Magnetic nanoparticles offer some properties that are attractive in the field of biomedical applications. Recently, ferrofluids (FFs) have been the subject of a great deal of interest because of their unusual optical, electronic, and magnetic properties, (Brojabasi, Muthukumaran, et al. 2015; Brojabasi, Mahendran, et al. 2015; López et al. 2014; Pu & Dong 2014; Pu & Liu 2009) which can be changed by applying an external magnetic field. However, the use of magnetic particles that are nanometer size has expanded their application in fields such as biomedicine. Such materials have been proposed, for example, as an alternative therapy for the localized treatment of malignant tumours; for this treatment, the nanoparticles are injected directly into the tumour. When FFs are placed in an alternating magnetic field, the nanoparticles generate heat and destroy the tumour. For medical applications, these materials must be biocompatible. Currently, FFs are promising materials for cancer diagnosis and therapy (Sakellari et al. 2015; Gas & Miaskowski 2015; Sharifi et al. 2012; Pankhurst et

al. 2009). Ferrofluids are colloidal systems composed of a single domain of magnetic nanoparticles with a mean diameter of approximately 10 nm dispersed in a liquid carrier. A special feature of FFs is the combination of a normal liquid behavior with super paramagnetic properties due to the small size of the particles. There are various methods to prepare magnetic nanoparticles in the nanometer size range due to their extensive technological applications (López et al. 2012; Scherer & Neto 2005; Anantharaman 2014). Currently, studies of cobalt zinc ferrite ($Co_{(1-x)}Zn_xFe_2O_4$.) spinels are of great interest due to the low coercivity and high saturation magnetization of this material. This magnetic behavior is appealing for a wide range of applications, such as biomedicine and nanophotonics, among others. In the present work, magnetic $Co_{(1-x)}Zn_xFe_2O_4$ ferrite nanoparticles were prepared using a co-precipitation method with aqueous salt solutions in an alkaline medium, and a study of their structure, morpholgy and magnetic properties was conducted.

EXPERIMENTAL DETAILS

The physical properties of nanoparticles in ferrofluid depend on the synthesis method and on the control of parameters such asthe reaction temperature, the pH of the suspension, the type of surfactant, the initial molar concentration, and others during the synthesis. Ferrofluids based on $Co_{(1-x)}Zn_xFe_2O_4$ magnetic nanoparticles were prepared using a previously reported chemical co-precipitation method (Guo et al. 2015; Xie 2012). The complete synthesis process for obtaining $Co_{(1-x)}Zn_xFe_2O_4$ magnetic nanoparticles at different $Zn_{(x)}$ concentration valueswas described by J. Lopez et al. (López et al. 2012). The morphology of the samples was characterized using scanning electron microscopy (SEM). SEM images were collected with a Philips XL30 ESEM that used a micro energy dispersive spectrometer EDS probe for the chemical analysis (12 kV) and that was equipped with a window to detect light elements. For crystal structure characterization, we performed X-ray diffraction (XRD) usingthe powder method in Bragg Brentano geometry and a Panalytical X'Pert-XRD diffractometer using the Cu K_α line (λ=1.548 Å, 45 kV and 40 mA) with a Ni-filter to remove the Cu K_β line. Patterns were recorded at room temperature in the range of 10° to 90° in the 2θ configuration with a 0.02° step. The Bragg peaks in the diffraction pattern were indexed and analyzed using the ICDD-PDF2 (International Centre for Diffraction Data) database and were compared with existing standards for the $ZnFe_2O_4$ and $CoFe_2O_4$ ferrites. We performed the Rietveld refinement using the GSAS program to obtain quantitative information about the crystal structure and crystallite size. Moreover, a lanthanum hexaboride (LaB_6) calibration sample was used for the diffraction pattern refinement to determine the difractometer instrumental broadening.

The magnetic properties of the nanoparticles in the ferrofluid were performed in a physical property measurement system (PPMS) of Quantum Design using the vibrating sample magnetometer (VSM) mode. The hysteretic magnetization loops were measured at room temperature by varying the applied field in the range between -20000 and 20000 Oe. For magnetic measurements, the ferrofluid samples were diluted in toluene at different volumetric concentrations (10%, 25%, 50%, or 75%) and were encapsulated in a sample holder. To study the type of predominant interaction between the particles, we used the Thamm - Hesse (THM) method fitting magnetization as a function of the applied field curves. We also performed measurements of zero field cooling (ZFC) and field cooling (FC) for thermal demagnetization curves between 4 K and 340 K with an applied field of 100 Oe. In both cases, the ZFC and FC data were measured using the same applied field.

RESULTS AND DISCUSSIONS

Scanning Electron Microscopy (SEM)

The scanning electron microscopy (SEM) allows the morphological characterization of $Co_{(1-x)}Zn_xFe_2O_4$ magnetic nanoparticles present in the ferrofluid. Figure 1 shows an SEM image of the sample with the highest Zn concentration ($Co_{0.25}Zn_{0.75}Fe_2O_4$), in which we can see clearly the presence of nano-sized clusters composed of much smaller spheroidal particles with average particle sizes between 10 and 28 nm (López et al. 2014; Zipare et al. 2015; Khalkhali et al. 2015). This observation indicates that, after the preparation of the samples for SEM observation, they exhibit the formation of particle aggregates or clusters with sizes in the nanometer range. Thus, it is not possible to find information about average size distribution of our nanoparticles using this technique. The manner in which these nanoparticles are grouped to form conglomerates or aggregates is by small contact areas that allow the gradual formation of particles with a larger size. This phenomenon may occur because nanoparticles in the conglomerate experience different interactions, such as surface tension and the steric effects of the surfactant material, as well as magnetic interaction.

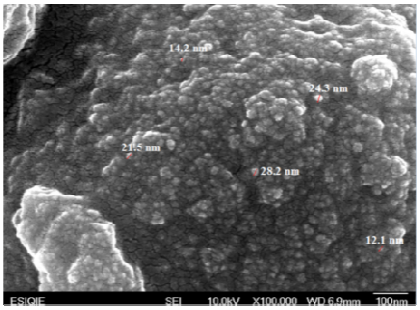

Figure 1: SEM Image of $Co_{0.25}Zn_{0.75}Fe_2O_4$ Magnetic Nanoparticles

Structural and Particle Characterization

Using the X-ray diffraction patterns analysis, we determined the crystal structure, lattice parameters, and crystal size for all the samples. **Figure 2** shows the diffraction patterns for the following Cobalt-Zinc ferrites: a) $CoFe_2O_4$; b) $Co_{0.75}Zn_{0.25}Fe_2O_4$; and c) $Co_{0.25}Zn_{0.75}Fe_2O_4$. Black symbols correspond to the experimental data, the red line corresponds to the refinement calculated difractogram, and the green line corresponds to the experimental calculated difference. It is clear that the reflection of the most intense peak appears in **Figure 2**, which corresponds to the crystallographic plane orientation (311). This indicates the formation of the spinel phase, characteristic for this type of ferrites (López et al. 2012; Mathew & Juang 2007; Javier A. Lopez, Ferney González, Flavio A. Bonilla, Gustavo Zambrano 2010; Lopez et al. 2012). The indexed (111), (220), (311), (222), (400), (422), (511) and (440) diffraction planes correspond to the characteristic cubic unit cell for the cobalt ferrite inverse spinel structure (Khalkhali et al. 2015; Munjal et al. 2016; Kim et al. 2003; Rekhila et al. 2016; Reddy & Yun 2016) at 2θ angles of approximately 21.4°, 35.12°, 41.42°, 50.32°, 62.72°, 67.22° and 74.06°. These crystallographic orientations are characteristic of $ZnFe_2O_4$ and $CoFe_2O_4$ ferrites. Moreover, these peaks are shifted slightly to the left as the Zn concentration increases. These results are consistent with the diffraction patterns reported in previous studies (López et al. 2012; Javier A. Lopez, Ferney González, Flavio A. Bonilla, Gustavo Zambrano 2010; Lopez et al. 2012; Arulmurugan et al. 2005). In the spinel structure (AB_2O_4), the peak intensity corresponding to the (220) planes in those crystallites depends exclusively on the cations occupying the tetrahedral sites *A*. The apparent changes in the intensities of the (220) planes indicate that the concentration of cations in position *A* decreases while the concentration at the *B* sites (octahedral sites) increases; that is, the cations migrate from the tetrahedral sites to the octaedral sites.

Additionally, considering the structural formulas of $[Zn]_T[Fe]_{2O}O_4$ for zinc ferrite and $[Fe]_T[Co, Fe]_OO_4$ for cobalt ferrite proposed by W. Fontjin et al.(Fontijn et al. 1999), it is possible to explain the migration of Zn, Co and Fe ions when the Zn concentration varies (x value changes) in the $Co_{(1-x)}Zn_xFe_2O_4$ system(Jnaneshwara et al. 2014; Wang et al. 2013; Malik et al. 2014). When Zn is added to the system (or Co decreases), Zn ions begin to occupy the sites of the Fe ions that are located in the tetrahedral sites. These Fe ions migrate into the octahedral sites, displacing Co ions; thus, the system experiences a structural transformation from a spinel inverse to normal spinel.

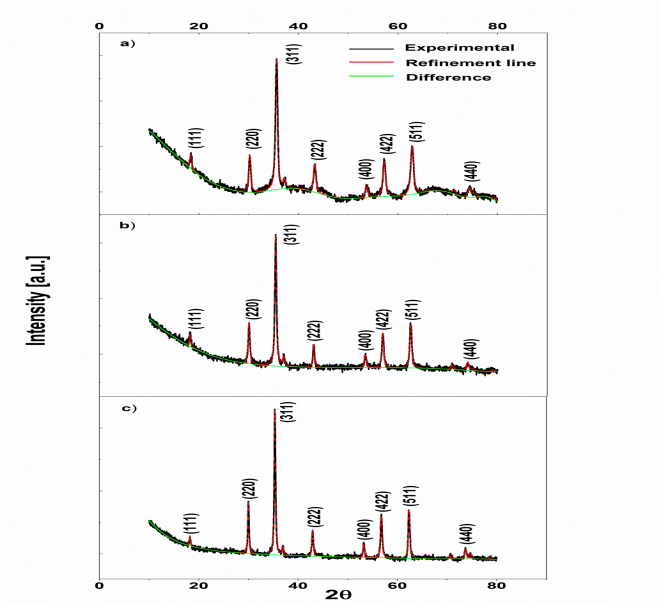

Figure 2: X-Ray Diffraction Patterns for a) $Cofe_2o_4$, b) $Co_{0.75}Zn_{0.25}Fe_2O_4$, and c) $Co_{0.25}Zn_{0.75}Fe_2O_4$ Ferrites. Black Symbols Are the Experimental Data; The Red Line is the Refinement Curve; The Green Line is the Experimental Calculated Data Difference.

This process causes the Bragg peaks to intensify and to shift slightly towards larger angles (Fontijn et al. 1999), as shown in **Figure 2**. The crystallite size and lattice parameter values for $CoFe_2O_4$ and $Co_{(1-x)}Zn_xFe_2O_4$ ferrites are shown in **Table 1**. The lattice parameter increases with the increasing substitution of Co for Zn ions in the unit cell. According to the above discussion, Zn ions prefer to occupy the tetrahedral sites, which are smaller than the octahedral sites, due to the larger atomic radius of Zn compared to Co. This causes the network to expand, thereby increasing the lattice parameter value without disturbing the symmetry of the unit cell (López et al. 2012; Jnaneshwara et al. 2014; Malik et al. 2014). Likewise, the average crystallite size of samples determined by the Rietveld refinement decreases with the increasing concentration of zinc, indicating that it is possible to have a control over the crystallite size by varying the stoichiometry of the ferrites. The crystallite size obtained from the results of the refinement was calculated according to the following (Dreele 2004; Vogel 2011) expressions:

$$\Phi_{per} = \frac{(18000)K\lambda}{\pi L_x} \quad \Phi_{par} = \frac{(18000)K\lambda}{\pi(L_x + ptec)} \tag{1}$$

where L_x corresponds to the Lorentzian isotropic crystallite size broadening, *petec* corresponds to the Lorentzian anisotropic crystallite size broadening, $K = 0.9$ is the Scherrer constant, and λ is the incidentradiation wavelength (Safi et al. 2016). **Table 1** also shows the L_x and *petec* parameter values obtained from the refinement used to determine the crystal size as well as the lattice parameter for the Co–Zn ferrite nanoparticles. In addition, the size effects of magnetic

nanoparticle systems are closely related to the fact that the volume of the nanoparticles is small (tens of nm^3), thus having an influence on their physical properties, such as magnetic and crystalline behavior.

Table 1: Refinement Parameter Values Obtained from the XRD Diffraction Patterns for the Nanoparticles of Co – Zn Ferrites

Sample	Lx [±0.01Å]	Petec [±0.18Å]	Crystal size [nm]	LatticeParameter [Å]
CoFeO	2.35	- 1.71 x 10^{-1}	33.7 ±0.2	8.369 ±0.002
$Co_{0.75}Zn_{0.25}Fe_2O_4$	3.16	1.24 x 10^{-1}	25.1 ±0.3	8.403 ±0.003
$Co_{0.25}Zn_{0.75}Fe_2O_4$	3.82	8.18x 10^{-3}	20.8 ±0.2	8.432 ±0.002

Hysteresis Loops for Co – Zn Ferrite Magnetic Nanoparticles

Figure 3 shows the hysteresis magnetization loops for **(a)** $Co_{0.25}Zn_{0.75}Fe_2O_4$and **(b)** $Co_{0.75}Zn_{0.25}Fe_2O_4$ samples at different volume concentrations (10%, 25%, 50% and 75%) of nanoparticles dispersed in toluene as the carrier liquid. We observe that samples exhibit the typical behavior of a soft magnetic material: low coercive field (superparamagnetic material) and a monotonic increase of magnetization until saturation. This indicates the presence of an ordered magnetic structure for this type of mixed ferrite. On the other hand, when we change the composition from $Co_{0.75}Zn_{0.25}Fe_2O_4$ to $Co_{0.25}Zn_{0.75}Fe_2O_4$ (Figure 3a and 3b), the saturation magnetization increases because we are replacing the magnetic atoms (Co) with non-magnetic atoms (Zn). Moreover, if the concentration of ferrofluid increased from 10% to 75% for the same volume of carrier liquid, the saturation magnetization increases while the coercive field decreases, as shown in **Figure 3 (c)** for the $Co_{0.25}Zn_{0.75}Fe_2O_4$ sample. This behavior occurs due to the presence of a larger number of magnetic moments that align with the external magnetic field and that contribute to the net magnetization of the material in the presence of the applied field. We could associate the increase of the saturation magnetization with the fact that the non-magnetic Zn^{2+} ion has a preferred occupation of *A* sites replacing the magnetic atom Fe^{3+} in *B* sites. This behavior also can be due to a super exchange interaction between the *A* and *B* sites within the spinel structure, which produces an increase in the magnetization(López et al. 2012; Malik et al. 2014).

The magnetization loops for our ferrofluid samples have coercivity and saturation values that depend on the particle sizes. It is known that magnetic particles can be considered as a magnetic single-domain when the sizes are below 100 nm. In contrast, for sizes less than 30 nm, particles tend to exhibit super paramagnetic behavior, assuming that the particles are monocrystalline. In our case, the $Co_{0.75}Zn_{0.25}Fe_2O_4$ and $Co_{0.25}Zn_{0.75}Fe_2O_4$ particle sizes are 24.9 and 13.2 nm, respectively (López et al. 2014; López et al. 2012; Lopez Medina et al. 2016). Therefore, the very low coercive field in the magnetization loops indicates that these magnetic nanoparticles can be considered as a single-domain particle with a tendency of super paramagnetic behavior at room temperature. The $Co_{0.75}Zn_{0.25}Fe_2O_4$ sample with the highest ferrofluid volume concentration (75%) has a coercive field of H_c = (40 ± 0.2) Oe and a saturation magnetization of 0.36 emu/g; while the $Co_{0.25}Zn_{0.75}Fe_2O_4$ sample with the highest ferrofluid concentration exhibits H_c = (7 ± 0.2) Oe and a saturaton magnetization of 0.69 emu/g. The lower coercive field and the higher saturation magnetization for the sample with the highest concentration of zinc ($Co_{0.25}Zn_{0.75}Fe_2O_4$ ferrite) indicate that the Co^{2+} ions are being replaced by nonmagnetic Zn^{+2} ions in the mixed ferrite. Thus, the magnetic properties of the samples are highly dependention the stoichiometry of the nanoparticles for ion substitution in the unit cell Table 2 summarizes the structural (lattice parameter, crystallite size and nanoparticle size) and magnetic (coercive field and saturation magnetization) results obtained from the XRD and VSM measurements for the three stoichiometries. We can infer from the data that there is a strong dependence of the Zn

concentration or the partial Co replacement on the decrease of the coercive field H_c, nanoparticle size and the crystallite size.

Table 2: Crystallite and Nanoparticle Size Values, Lattice Parameters and Coercive Field Values for the Co - Zn Ferrites

Sample	Lattice Parameter [Å]	Crystal size [nm]	Coercive Field [± 1 Oe]	Saturation magnetization [± 1 emu/g]	D_N [± 0.1 nm]
CoFeO	8.369 ±0.002	33.7 ±0.2	593	1.09	28.7
$Co_{0.75}Zn_{0.25}Fe_2O_4$	8.403 ±0.003	25.1 ±0.3	40	0.36	24.9
$Co_{0.25}Zn_{0.75}Fe_2O_4$	8.432 ±0.002	20.8 ±0.2	7	0.69	13.2

The magnetic behavior can be explained by the fact that, in the spinel structure, the magnetic order is primarily due to the mechanism of an exchange interaction caused by the metal ions that occupy the *A* and *B* sites in the crystal structure. Partial substitution with diamagnetic ions such as Zn will result in a preferential occupancy of the *A* sites. Thus, there is a reduction in the exchange interaction between the *A* and *B* sites; i.e., by varying the degree of zinc substitution, the magnetic properties of the nanoparticles can be modulated. This effect it is observed in the decrease of the coercive field values. Therefore, by replacing Co with a Zn ion, the particle size is reduced and the trend toward super paramagnetic behavior at room temperature is promoted (López et al. 2014; Fontijn et al. 1999; Malik et al. 2014; Vaidyanathan & Sendhilnathan 2008). Weak hysteresis (very small coercivity) could be attributed to the fact that the magnetic moments of the nanoparticles are free to fluctuate as a whole in response to the thermal energy present; the individual atomic moments remain in an orderly state relative to each other, thus exhibiting super paramagnetic behavior, which it is characteristic of magnetic nanoparticle systems.

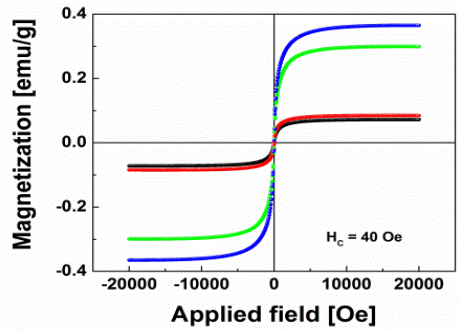

a)

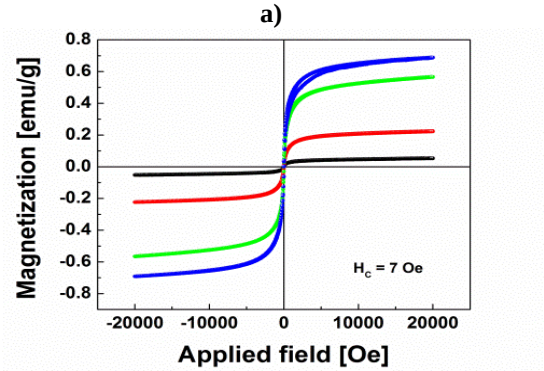

b)

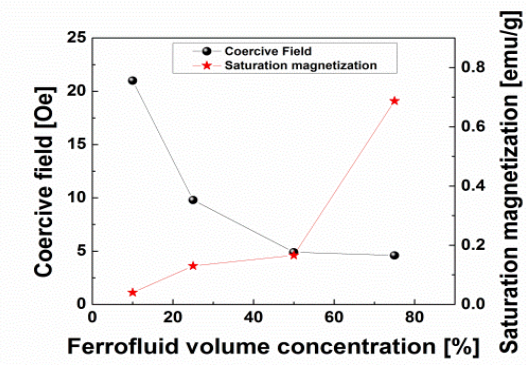

c)

Figure 3: Hysteresis Loops at Room Temperature for the Ferrofluids a) $Co_{0.75}Zn_{0.25}Fe_2O_4$ and b) $Co_{0.25}Zn_{0.75}Fe_2O_4$; Ferrite magnetic nanoparticles at Ferrofluid Volume Concentrations of 10% (Black Symbol), 25% (Red Symbol), 50% (Green Symbol) or 75% (Blue Symbol). c) Percent Ferrofluid Volume Concentration Dependence of the Coercive Field (Round bLack Symbol) and Saturation Magnetization (Round Red Symbol) for the $Co_{0.25}Zn_{0.75}Fe_2O_4$ Sample

Thamm – Hesse Analysis for Co – Zn Ferrite

To study the magnetic interaction existing between the magnetic nanoparticles in the samples of ferrofluid, the Thamm–Hesse (THM) method was used. In 1996, Thamm and Hesse proposed a simple graphic that uses the diference between the initial magnetization curve and the average value for the other two branches of the curve (ΔM) for a single-domain particles system to study the magnetic interactions between each of them. The mechanism used to describe the hysteresis curve is the following: the hysteresis loop data are divided into five sections of equal length, from 0 – H_{max}(initial curve), H_{max}– 0 (upper curve), 0 –H_{max} (which is not taken into account), – H_{max} – 0 (also excluded from analysis) and de 0 – H_{max} (bottom curve). The following equation is used to determine the Thamm-Hesse deviation ($\Delta M_{Thamm–Hesse}$) for the ΔM graph (Thamm & Hesse 1996; Stefan Thamm and Jurgen Hesse 1998; Chwastek 2010; Michele et al. 2004; Aslibeiki 2016):

$$\Delta M_{\text{Thamm-Hesse}}(B)=M_{\text{inicial}}-\frac{M_{\text{superior}}+M_{\text{inferior}}}{2} \quad (2)$$

The data are plotted as a function of the external magnetic field for the values of 0 - H_{max} for ideal particles of the Stoner-Wohlfarth type (single domain particles with uniaxial anisotropy and noninteracting). It is expected that the plotted data for ΔM tend towards zero to establish the super paramagnetic character for such particles. The Stoner-Wohlfarth model also assumes coherent rotation, which is the simplest way to describe the physics for the fine magnetic particles adequately containing single domains and to study the behavior of the magnetization as a function of the applied magnetic field. In addition, this is also the basis for applying the THM to establish the type of magnetic interaction existing within a sample of magnetic particles if any of the following conditions take place. If ΔM=0, the system is superparamagnetic or paramagnetic. For ΔM ≠ 0, there are interactions between the particles or grains. In the case that ΔM > 0, interactions that favor magnetization prevail (exchange interaction). Finally, if ΔM < 0, interactions that favor magnetization reversal prevail (dipolar interaction). **Figure 4** shows the THM plots for the ferrites $Co_{0.75}Zn_{0.25}Fe_2O_4$ and $Co_{0.25}Zn_{0.75}Fe_2O_4$. In this case, the interactions that favor the magnetization reversal (dipolar interaction) for different volume concentrations of ferrofluid prevail for magnetic field values between 0 and 4 kOe. As the magnetic field increases, the interactions that favor the magnetization (exchange interaction) begin to prevail, i.e., the magnetic moments start to align with the applied

field direction. In contrast, the sample with 10% ferrofluid volume presents a very intense peak for lower fields in the region where the exchange interactions prevail, which indicates that it favors the easy magnetization along the easy axis. This effect can be attributed to the fact that this sample did not have sufficient diluted magnetic nanoparticles in the ferrofluid. Whereas, for the sample with 75% ferrofluid volume, the peak that appears in the same region is less pronounced due to the higher concentration of magnetic nanoparticles in the sample, and their magnetic moments are aligned along the direction of the applied field promoting the magnetization of the system. Finally, in the case of magnetic fields greater than 5 kOe, a slight decay appears for the curve with values close to zero, indicating that interactions that favor the superparamagnetic behavior for magnetic nanoparticles present in the ferrofluid. Thus, the nanoparticles of $Co_{(1-x)}Zn_xFe_2O_4$ ferrite obtained via the chemical coprecipitation method widely satisfy the Stoner-Wohlfarth model because the ΔM values tend toward zero. In other words, it can be confirmed that it is not possible to make the particles exhibit interactions that favor the magnetization exchange or magnetization reversal at high magnetic field values. The same effects are observed for the other two concentrations (25% and 50%) of ferrofluid volume.

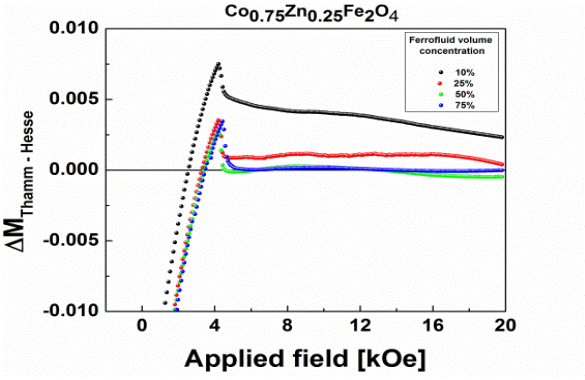

a)

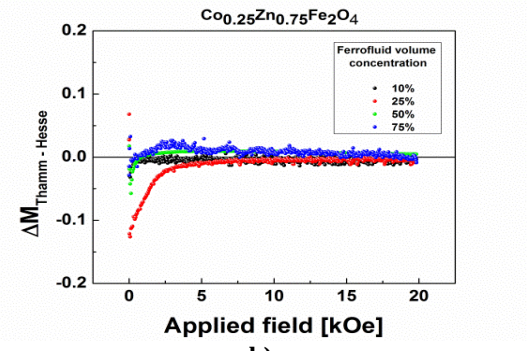

b)

Figure 4: Thamm–Hesse Analysis for Magnetic Nanoparticles in the Ferrofluids a) $Co_{0.75}Zn_{0.25}Fe_2O_4$ and b) $Co_{0.25}Zn_{0.75}Fe_2O_4$

ZFC and FC Magnetization Study of Co – Zn Ferrites

To study the nanoparticle size, blocking temperature (T_B) measurements of the FC (Field Cooling) and ZFC (Zero Field Cooling) processes for Co – Zn magnetic nanoparticles dispersed in the carrier liquid were made. Figure 5 (a) and (b)**,** we plotted the magnetization as a function of temperature between 4 K and 300 K with a constant applied field of 100 Oe. From the FC and ZFC curves, one can observe the irreversibility of magnetization, a typical behavior of the blocking process of super paramagnetic nanoparticles (Socolovsky et al. 2003). In Figure 5, the peak of the curve at a given temperature (below room temperature) corresponds to the T_B. In the case of $Co_{0.75}Zn_{0.25}Fe_2O_4$ and $Co_{0.25}Zn_{0.75}Fe_2O_4$

ferrites, the T_B values were 163 K and 106 K, respectively. Above this magnetization value, the T_B decreases as the temperature increases. From the behavior of the ZFC and FC curves, it is possible to assert that these curves almost overlap above the T_B, indicating the presence of small-sized particles. The ZFC magnetization curves were fitted using a system of non-interacting spherical nanoparticles with a volume distribution of approximately V_o. The procedure used to fit the ZFC mesurements is fully described in the work of J. Lopez et al. (López et al. 2012) and is applied to obtain the critical volume value of the nanopaticles and to determine their critical diameter. It is known that the critical volume of the nanostructured superparamagnetic materials is directly proportional to the blocking temperature (Socolovsky et al. 2003; Knobel et al. 2004; M. Knobel, W. C. Nunes, L. M. Socolovsky, E. De Biasi 2008; Blanco-Gutiérrez et al. 2016; Eun Choi, Y Ahn 2008; Dipietro et al. 2010). Thus, when the temperature increases, the critical size of the particles will be greater, and the particles of a size less than or equal to the critical value can be considered to belong to the superparamagnetic regime. In addition, the V_c value allows the determination of the critical diameter for the nanoparticles, assuming a spherical geometry.

In **Figure 5** (a) and (b), the irreversibility temperature corresponds to the temperature, where the ZFC magnetization curve is separated from the FC curve. In addition, the derivative with respect to the temperature of the difference between the FC and ZFC curves as a temperature function is presented. These plots provide information about the size distribution profile of the nanoparticles and obey a lognormal distribution function. In this case, from the distribution of sizes and using a fit to the lognormal function, the T_B, V_c and D_c values obtained for the $Co_{0.75}Zn_{0.25}Fe_2O_4$ and $Co_{0.75}Zn_{0.25}Fe_2O_4$ samples were T_B = 20 and 45 K, respectively, V_c = 79.3 and 151.7 nm^3, respectively, and D_c = 5.4 and 6.6 nm, respectively. The critical diameter values for the nanoparticles are consistent with the crystal sizes obtained from the XRD measurements.

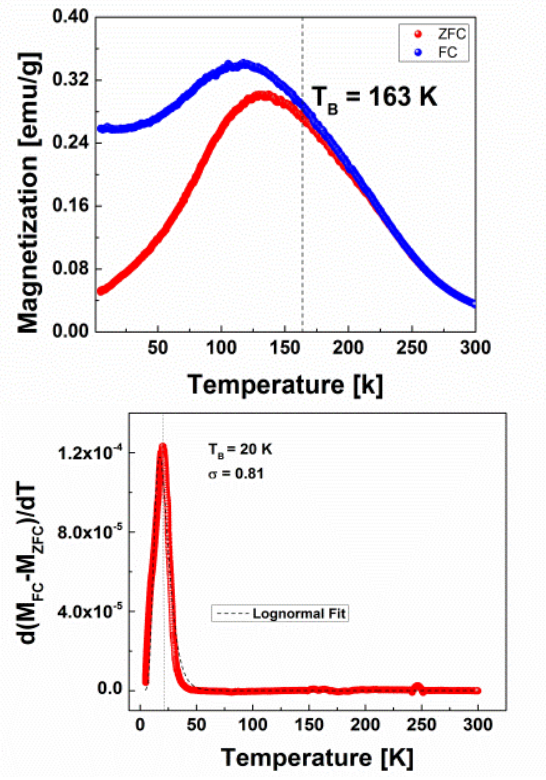

a)

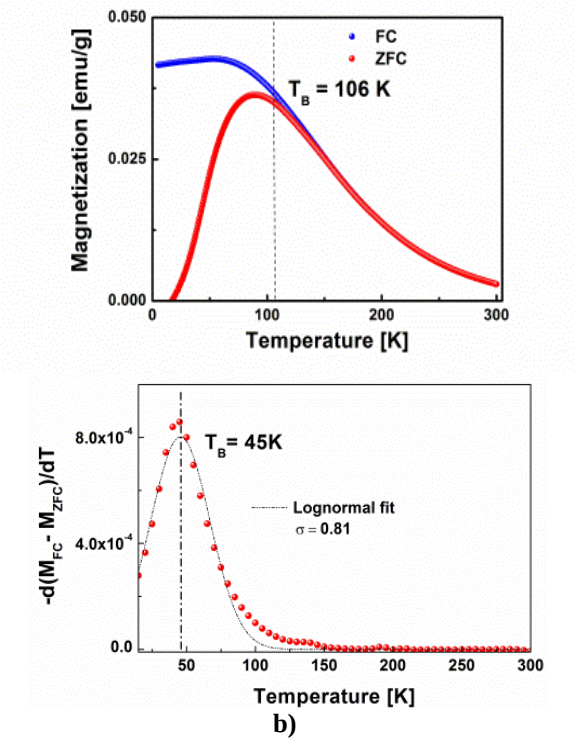

b)

Figure 5: ZFC and FC Magnetization (Left) Versus Temperature Plots for a) $Co_{0.75}Zn_{0.25}Fe_2O_4$ and b) $Co_{0.25}Zn_{0.75}Fe_2O_4$. Plots at the Right Are the Derivative of the Difference between the ZFC and FC Curves as a Function of Temperature.

Finally, this type of system shows an interesting behavior when confined to a fluid film cell with a low thickness (~10 nm) and placed under an external magnetic field. In fact, the magnetic nanoparticles formed chains or magnetic columns, depending of the direction of the applied field to the sample. When a perpendicular magnetic field is applied, the nanoparticles form magnetic rods. In contrast, if the magnetic field is applied parallel, it is possible to obtain magnetic chains. In both cases, the columns or chains can be modulated by the magnetic field. These effects are directly related to the film thickness and the strength of the applied field. The above behaviors allow the consideration of these systems as soft materials with magneto-controllable properties for applications in the potential development of photonic devices. **Figure 6** shows the optical images of a magnetic fluid film under the action of parallel or perpendicular magnetic fields; magnetic chains (needles) or magnetic columns are formed by nanoparticles of Co–Zn ferrites. When the magnetic field is applied to the magnetic fluid cell, the magnetic moments of nanoparticles present in the ferrofluid begin to align with the magnetic field direction and to self–assemble to form different patterns, such as hexagonal patterns or one-dimensional periodic chain structures (López et al. 2014; Pu & Dong 2014; Lopez Medina et al. 2016; Yu et al. 2013).

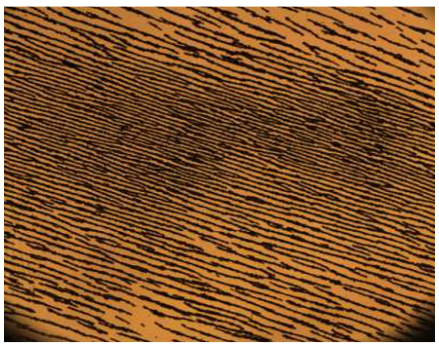

a)

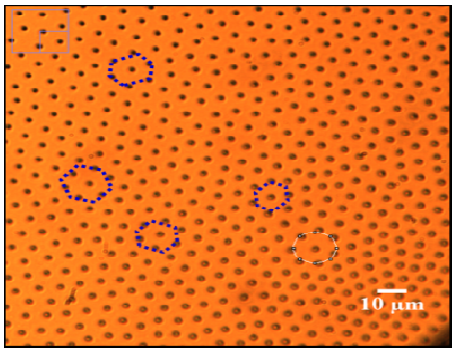

b)

Figure 6: Optical Images for the Self Assembly of the Co $_{(1-X)}$ Znxfe2o4 Magnetic Nanoparticles Confined in a Fluid Film Cell under the Action of a) Parallel or b) Perpendicular External Magnetic Fields at Room Temperature

CONCLUSIONS

XRD analysis was used to show the presence of the characteristic spinel structure in $Co_{1-x}Zn_xFe_2O_4$ ferrofluid nanoparticles. It was also shown that the crystal and conglomerate sizes determined by XRD decrease with the increase of Zn at %. Hence, decreasing the size of nanoparticles by cobalt zinc substitution may be ideal for various technological applications. In addition, $Co_{1-x}Zn_xFe_2O_4$ magnetic nanoparticles exhibit super paramagnetic behavior, resulting in a decrease of the coercive field of the $Co_{1-x}Zn_xFe_2O_4$ magnetic nanoparticles with the increase of Zn at%. In summary, the $Co_{(1-x)}Zn_xFe_2O_4$ferrofluids prepared by the coprecipitation method showed super paramagnetic behavior, which was documented by the hysteresis loop measured at room temperature. Therefore, our magnetic nanoparticles can be considered as a soft magnetic material with interesting technological applications in nanotechnology; ferrofluids based on magnetic nanoparticles that, under the action of an external magnetic field, show optical properties that are make them are interesting as a magnetically tunable device.

ACKNOWLEDGEMENTS

This work was supported by COLCIENCIAS through the 1106-658 42312 project under Contract 6242014 and partially by the Center of Excellence for Novel Materials, *Universidad del Valle*.

REFERENCES

1. Anantharaman, S.N. and M.R., 2014. Introduction to ferrofluids. *Chaos and Complexity Letters*, 7(1/2), pp.1–5
2. Arulmurugan, R. et al., 2005. Co-Zn ferrite nanoparticles for ferrofluid preparation: Study on magnetic properties. *Physica B: Condensed Matter*, 363(1–4), pp.225–231
3. Aslibeiki, B., 2016. Magnetic interactions and hysteresis loops study of Co/CoFe2O4 nanoparticles. *Ceramics International*, 42(5), pp.6413–6421
4. Blanco-Gutiérrez, V. et al., 2016. Temperature dependence of superparamagnetism in CoFe 2 O 4 nanoparticles and CoFe 2 O 4 /SiO 2 nanocomposites. *Phys. Chem. Chem. Phys.*, pp.9186–9193
5. Brojabasi, S., Mahendran, V., et al., 2015. Temperature dependent light transmission in ferrofluids. *Optics Communications*, 342, pp.224–229
6. Brojabasi, S., Muthukumaran, T., et al., 2015. The effect of suspended Fe3O4 nanoparticle size on magneto-

optical properties of ferrofluids. *Optics Communications*, 336, pp.278–285.

7. Chwastek, K., 2010. Description of Henkel plots by the magnetization-dependent Jiles-Atherton model. *Journal of Magnetism and Magnetic Materials*, 322(2), pp.214–217
8. Dipietro, R.S. et al., 2010. Determining magnetic nanoparticle size distributions from thermomagnetic measurements. *Applied Physics Letters*, 96(22).
9. Dreele, A.C.L. and R.B. Von, 2004. General Structure Analysis System (GSAS). *Los. Alamos National Laboratory Report (LAUR)*, 748, pp.86–748
10. Eun Choi, Y Ahn, E.. H., 2008. Size dependence of the magnetic properties in superparamagnetic zinc-ferrite nanoparticles. *Journal of Korean Physical Society*, 53(4), pp.2090–2094
11. Fontijn, W.F.J. et al., 1999. A consistent interpretation of the magneto-optical spectra of spinel type ferrites (invited). *Journal of Applied Physics*, 85(8), p.5100
12. Gas, P. & Miaskowski, A., 2015. Specifying the ferrofluid parameters important from the viewpoint of Magnetic Fluid Hyperthermia. *Selected Problems of Electrical Engineering and Electronics, IEEE Xplore Digital Library*, pp.1–6
13. Guo, T., Bian, X. & Yang, C., 2015. A new method to prepare water based Fe 3 O 4 ferrofluid with high stabilization. *Physica A*, 438(xxxx), pp.560–567
14. Javier A. Lopez, Ferney González, Flavio A. Bonilla, Gustavo Zambrano, M.E.G., 2010. Synthesis and characterization of Fe 3 O 4 magnetic nanofluid. *Revista Latinoamericana de Metalurgia y Materiales*, 30(1), pp.60–66
15. Jnaneshwara, D.M. et al., 2014. Effect of zinc substitution on the nanocobalt ferrite powders for nanoelectronic devices. *Journal of Alloys and Compounds*, 587, pp.50–58
16. Khalkhali, M. et al., 2015. The impact of polymer coatings on magnetite nanoparticles performance as MRI contrast agents: a comparative study. *Daru : journal of Faculty of Pharmacy, Tehran University of Medical Sciences*, 23(1), p.45
17. Kim, Y. Il, Kim, D. & Lee, C.S., 2003. Synthesis and characterization of CoFe2O4 magnetic nanoparticles prepared by temperature-controlled coprecipitation method. *Physica B: Condensed Matter*, 337(1–4), pp.42–51
18. Knobel, M., Socolovsky, L.M. & Vargas, J.M., 2004. Propiedades magnéticas y de transporte de sistemas nanocristalinos: conceptos básicos y aplicaciones a sistemas reales. *Revista Mexicana de Física E*, 50(1), pp.8–28
19. López, J. et al., 2014. Magnetic field role on the structure and optical response of photonic crystals based on ferrofluids containing Co0.25Zn0.75Fe2O4 nanoparticles. *Journal of Applied Physics*, 115(19), p.193502
20. López, J. et al., 2012. Study of magnetic and structural properties of ferrofluids based on cobaltzinc ferrite nanoparticles. *Journal of Magnetism and Magnetic Materials*, 324(4), pp.394–402
21. Lopez, J., Espinoza-beltran, F.J. & Zambrano, G., 2012. Caracterización de nanopartículas magnéticas preparadas por el método de coprecipitación química. *Revista Mexicana de Física*, 58, pp.293–300

22. Lopez Medina, J.A. et al., 2016. Band Structure Dependence on the External Perpendicular Magnetic Field and Zn Concentration of Photonic Crystals Made of Co(1-x)ZnxFe2O4 Nanoparticles. *IEEE Transactions on Magnetics*, 52(1), pp.1–7

23. M. Knobel, W. C. Nunes, L. M. Socolovsky, E. De Biasi, J.M.V. and J.C.D., 2008. Superparamagnetism and Other Magnetic Features in Granular Materials: A Review on Ideal and Real Systems. *Journal of Nanoscience and Nanotechnology*, 8(4), pp.2836–2857. Available at: http

24. Malik, H. et al., 2014. Influence of cobalt substitution on the magnetic properties of zinc nanocrystals synthesized via micro-emulsion route. *Ceramics International*, 40(7 PART A), pp.9439–9444

25. Mathew, D.S. & Juang, R.S., 2007. An overview of the structure and magnetism of spinel ferrite nanoparticles and their synthesis in microemulsions. *Chemical Engineering Journal*, 129(1–3), pp.51–65

26. Michele, O. et al., 2004. Demagnetization experiments on frozen ferrofluids. *Physica Status Solidi C: Conferences*, 1(12), pp.3596–3602

27. Munjal, S. et al., 2016. Water dispersible CoFe2O4 nanoparticles with improved colloidal stability for biomedical applications. *Journal of Magnetism and Magnetic Materials*, 404, pp.166–169

28. Pankhurst, Q.A. et al., 2009. Progress in applications of magnetic nanoparticles in biomedicine. *Journal of Physics D: Applied Physics*, 42, p.224001

29. Pu, S. & Dong, S., 2014. Magnetic field sensing based on magnetic-fluid-clad fiber-optic structure with up-tapered joints. *IEEE Photonics Journal*, 6(4)

30. Pu, S. & Liu, M., 2009. Tunable photonic crystals based on MnFe2O4 magnetic fluids by magnetic fields. *Journal of Alloys and Compounds*, 481(1–2), pp.851–854

31. Reddy, D.H.K. & Yun, Y.-S., 2016. Spinel ferrite magnetic adsorbents: alternative future materials for water purification? *Coordination Chemistry Reviews*, 315, pp.90–111

32. Rekhila, G., Bessekhouad, Y. & Trari, M., 2016. Synthesis and characterization of the spinel ZnFe2O4, application to the chromate reduction under visible light. *Environmental Technology & Innovation*, 5, pp.127–135

33. Safi, R. et al., 2016. Rietveld structure refinement, cations distribution and magnetic features of CoFe2O4 nanoparticles synthesized by co-precipitation, hydrothermal, and combustion methods. *Ceramics International*, 42(5), pp.6375–6382

34. Sakellari, D. et al., 2015. Exploring multifunctional potential of commercial ferrofluids by magnetic particle hyperthermia. *Journal of Magnetism and Magnetic Materials*, 380, pp.360–364.

35. Scherer, C. & Neto, A.M.F., 2005. Ferrofluids : Properties and Applications. *Brazilian Journal of Physics*, 35(3), pp.718–727

36. Sharifi, I., Shokrollahi, H. & Amiri, S., 2012. Ferrite-based magnetic nanofluids used in hyperthermia applications. *Journal of Magnetism and Magnetic Materials*, 324(6), pp.903–915

37. Socolovsky, L.M., Knobel, M. & Vargas, J.M., 2003. Propiedades Magneticas De Sistemas Nanocristalinos:

Conceptos Basicos. *Revista Cubana De Fisica*, 20(1), pp.3–11

38. Stefan Thamm and Jurgen Hesse, 1998. The remanence of a Stoner—Wohlfarth particle ensemble as a function of the demagnetisation process. *Journal of Magnetism and Magnetic Materials*, 184, pp.245–255
39. Thamm, S. & Hesse, J., 1996. A simple plot indicating interactions between single-domain particles. *Journal of Magnetism and Magnetic Materials*, 154(2), pp.254–262
40. Vaidyanathan, G. & Sendhilnathan, S., 2008. Characterization of Co 1 À x Zn x Fe 2 O 4 nanoparticles synthesized by co-precipitation method., 403(1), pp.2157–2167
41. Vogel, S.C., 2011. gsaslanguage: a GSAS script language for automated Rietveld refinements of diffraction data. *Journal of Applied Crystallography*, 44(4), pp.873–877. Available at: http://scripts.iucr.org/cgi-bin/paper?cg5186 [Accessed April 8, 2016]
42. Wang, W. et al., 2013. Synthesis and characteristics of superparamagnetic Co 0.6 Zn 0.4 Fe 2 O 4 nanoparticles by a modified hydrothermal method. *Journal of the American Ceramic Society*, 96(7), pp.2245–2251
43. Xie, W.Y. and H., 2012. A Review on Nanofluids: Preparation, Stability Mechanisms, and Applications. *Journal of Nanomaterials*, 2012, pp.1–17
44. Yu, G.J. et al., 2013. Tunable one-dimensional photonic crystals based on magnetic fluids. *Optik*, 124(17), pp.2713–2715
45. Zipare, K. et al., 2015. Superparamagnetic Manganese Ferrite Nanoparticles : Synthesis and Magnetic Properties., 1(3), pp.178–182